Total and partial recombination cross sections for F^{6+}

D. M. Mitnik and M. S. Pindzola
Department of Physics, Auburn University, Auburn, Alabama 36849

N. R. Badnell
Department of Physics and Applied Physics, University of Strathclyde, Glasgow G4 0NG, United Kingdom
(Received 13 October 1998; revised manuscript received 6 January 1999)

Total and partial recombination cross sections for F^{6+} are calculated using close-coupling and distorted-wave theory. For total cross sections, close-coupling and distorted-wave results, which include interference between the radiative and dielectronic pathways, are found to be in good agreement with distorted-wave results based on a sum of independent processes. Total cross sections near zero energy are dominated by contributions from low-energy dielectronic recombination resonances. For partial cross sections, the close-coupling and distorted-wave theories predict strong interference for recombination into the final recombined ground state $1s^2 2s^2\,{}^1S_0$ of F^{5+}, but only weak interference for recombination into the levels of the $1s^2 2s 2p$ configuration. [S1050-2947(99)09205-7]

PACS number(s): 34.80.Lx

I. INTRODUCTION

The free-bound spontaneous radiative emission process plays an important role in the determination of the level populations and ionization balance of high temperature non-LTE laboratory and astrophysical plasmas. This process is conventionally described as involving either direct (nonresonant) radiative recombination (RR), which is the inverse of the ordinary (nonresonant) photoionization process, or two-step (resonant) dielectronic recombination (DR), which consists of a radiationless electron capture (accompanied by excitation of the initial ion, to form a doubly excited autoionizing state) followed by a spontaneous radiatively stabilizing transition to a bound state.

It has been pointed out in several scattering-theory investigations that the treatment of radiative and dielectronic recombination as two distinct, noninterfering processes is not strictly permissible within the framework of a rigorous quantum-mechanical theory; see, e.g., [1]. Over the years a number of theoretical approaches which unify the two recombination processes have been developed. A general perturbative projection operator approach [2–5] and nonperturbative *R*-matrix methods [6] and a radiative optical potential [7,8] have provided computational approaches that can be easily applied to any atomic ion.

Many experimental efforts using ion storage rings have been made in searches for observational evidence of interference effects in total recombination cross sections. The high resolution achieved by these devices allows one to map out resonance structures at the order of one-hundredth of one electron volt [9]. However, even under these conditions, the interference effects in the total recombination remain elusive. As has been pointed out by Badnell and Pindzola [5], the largest DR-RR interference effects are in the weakest lines, which are generally buried under the stronger resonances. For most weak lines, interference effects are further suppressed due to resonance decay to many final recombined states.

There are cases in total recombination cross sections, however, in which a weak resonance decays to only one level. An example of this kind of resonance has been given by Gorczyca *et al.* [10] for the Ar-like Sc^{3+} ion at low energies. Interference effects in the total recombination cross section are produced by the unusual resonance structures associated with the $3p^5 3d^2\,{}^2F$ terms in the recombined Sc^{2+} ion, which radiate almost exclusively to the ground levels $3p^6 3d\,{}^2D$. Schippers *et al.* [11] have investigated this recombination process, but the experiment does not allow for a conclusive test of the theoretical predictions. As has been pointed out by the authors, limitations on the accuracy of both the calculations and the experimental measurements are present for this ion.

Experimental efforts have also been made using ion traps to search for observational evidence of interferences in recombination. Although the ion trap experiments measure a mixture of ion stages, they have a decided advantage over ion storage rings in that they can monitor the photon emission. This allows them to measure partial recombination cross sections, that is, recombination to a particular final state. However, the low-energy resolution of these devices limits their application to very highly charged ions. The only observation of RR-DR interference to date was reported by Knapp *et al.* [12] in an ion trap experiment. For a mixture of different ions (U^{87+} to U^{90+}), the $KL_{12}L_3$ resonance manifold with emission of a 100 keV photon exhibits a marked asymmetry. The strength of the asymmetry was confirmed by calculations of the $KL_{12}L_3$ partial recombination corresponding to the emission of a 100 keV photon in U^{88+} ions [13].

In this paper we explore the possibility of finding interference effects in the total and partial recombination for low-charged atomic ions in the well-studied Li isoelectronic sequence. We calculate the total and partial recombination of F^{6+}, associated with the $1s^2 2pnl (n=6,7)$ configurations in the recombined F^{5+} ion. We confirm the general conclusion that substantial interference effects are not seen in the total recombination cross section. The most promising candidate for an observation of interference effects in the partial recombination cross section are the processes in which the

resonance decays to the lower $1s^2 2s^2\,{}^1S_0$ final recombined level. This partial recombination might be observed by counting the recombination events that occur simultaneously with an emission of light of approximately 150 eV.

In Sec. II we review nonperturbative and perturbative approaches for the photorecombinaton process. The nonperturbative theory is based on the *R*-matrix method for solving the coupled integro-differential equations which arise in the close-coupling approximation. The perturbative theory is based on the distorted-wave method. The perturbation expansion includes the sum of selected recombination terms through third-order. In Sec. III we present the total recombination cross section for F^{6+} in the energy range 0 eV to 4.5 eV, calculated by using both the perturbative and nonperturbative approaches. In Sec. IV we analyze the total recombination near zero energy. Examples of partial recombination which show asymmetric shapes are analyzed in Sec. V. Finally, the results are summarized in Sec. VI.

II. THEORY

Electron-ion recombination from level j into a particular final recombined level i, in the presence of one projectile continuum, may be schematically represented as

$$e^- + A_j^{q+} \rightarrow A_i^{(q-1)+} + h\nu \tag{1}$$

and

$$e^- + A_j^{q+} \rightleftharpoons A_n^{**(q-1)+} \rightarrow A_i^{(q-1)+} + h\nu, \tag{2}$$

where q is the charge on the atomic ion A, $h\nu$ is the energy of the emitted photon, and the double star in Eq. (2) indicates a doubly excited resonance level n. The first of these two pathways is called radiative recombination (RR) while the second is dielectronic recombination (DR).

By the use of the principle of detailed balance, the electric-dipole photorecombination cross section for an atomic ion in a level j to a recombined level i is given by (in atomic units)

$$\sigma_{j\rightarrow i}^R = \frac{g_i}{g_j}\frac{\omega^2}{c^2k^2}\sigma_{i\rightarrow j}^{\omega}, \tag{3}$$

where ω is the frequency of the radiation field, c is the speed of light, k is the linear momentum of the free electron, and g_i and g_j are the statistical weights of the final recombined ion level and of the initial target ion level, respectively. The photoionization cross section $\sigma_{i\rightarrow j}^{\omega}$, from level i to level j, is given by

$$\sigma_{i\rightarrow j}^{\omega} = \frac{4\pi^2 c^2}{\omega^2 k}|M_{i\rightarrow j}^{\omega}|^2, \tag{4}$$

where $M_{i\rightarrow j}^{\omega}$ is the photoionization matrix element of the corresponding transition given by

$$M_{i\rightarrow j}^{\omega} = \langle \psi_j | D | \psi_i \rangle, \tag{5}$$

and ψ_i is the initial bound state, ψ_j is the final state of the ionized ion plus continuum electron normalized to one times a sine function with energy $k^2/2$, and D is the dipole radiation field interaction in the length gauge:

$$D = \sqrt{(2\omega^3/3\pi c^3)}\sum_{s=1}^{N+1}\vec{r}_s. \tag{6}$$

The initial bound state ψ_i can be represented in both the perturbative and the nonperturbative approaches as a linear combination of different target configurations. We include, for example, configuration interaction between the $1s^2 2s^2$ and $1s^2 2p^2$ configurations in the present Li-like ion calculations.

The final state ψ_j is computed in a nonperturbative approach by solving the coupled integro-differential equations which arise in the close-coupling approximation [14]. This approach can be implemented by using the standard internal region *R*-matrix codes [15,16] and the external region *R*-matrix code developed by Seaton and co-workers (see, for example, Ref. [15]). We use here an extensively modified version of these codes written by Badnell *et al.* [17]. The close-coupling approach automatically includes many interference processes, such as interferences between resonances through the continuum, and between the resonances and with the nonresonant photoionization background. Furthermore, modified versions of the *R*-matrix codes can incorporate radiation damping via an imaginary optical potential [7].

A computationally faster approach for recombination is based on a perturbation method using distorted waves. In that case, the final state ψ_j is represented by a distorted wave coupled to a target wave function. In order to include interference effects in this approach, it is necessary to calculate higher-order terms in the perturbative expansion. The modifications to the first-order expression for the photoionization process due to the presence of resonances may be derived using either bound-continuum configuration-interaction theory [18] or diagrammatic many-body perturbation theory [19]. The contribution from a single autoionizing resonance ϕ_n yields the following modified matrix element:

$$M_{i\rightarrow j}^{\omega} = \langle \psi_j | D | \psi_i \rangle + \frac{\langle \psi_j | V | \phi_n \rangle \langle \phi_n | D | \psi_i \rangle}{\Delta_n + i\Gamma_n/2} + \langle \psi_j | D | \psi_i \rangle \left(-i\frac{A_{n\rightarrow j}^a/2}{\Delta_n + i\Gamma_n/2} \right). \tag{7}$$

In this expression Γ_n is the width of the ϕ_n resonance state and $\Delta_n = E - E_n$ is the energy detuning from resonance. The electron-electron interaction is given by

$$V = \sum_{s=1}^{N} |\vec{r}_s - \vec{r}_{N+1}|^{-1}, \tag{8}$$

and $A_{n\rightarrow j}^a$ is the autoionization rate from the autoionizing state n to the final state j

$$A_{n\rightarrow j}^a = \frac{4}{k}|\langle \psi_j | V | \phi_n \rangle|^2. \tag{9}$$

The second term in Eq. (7) represents a photoexcitation-autoionization process, which is the inverse of the dielec-

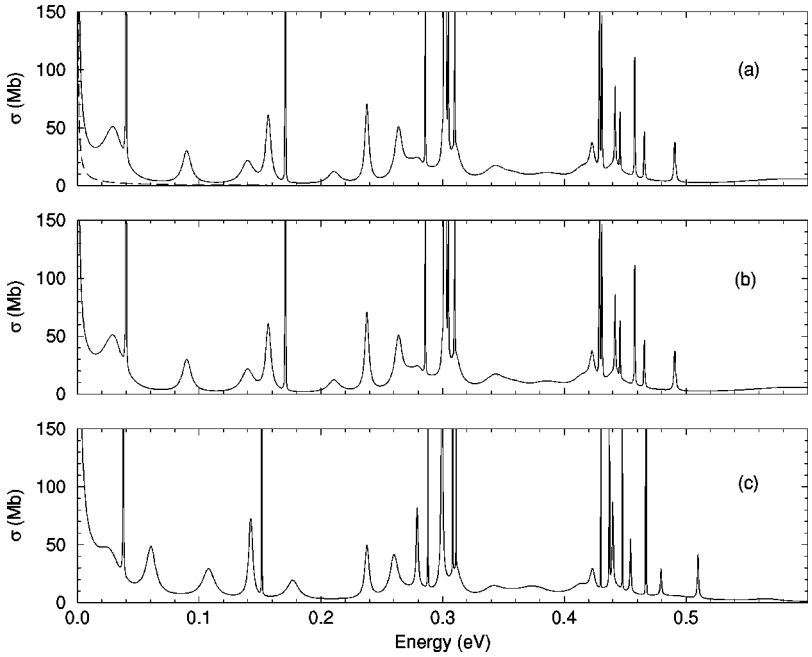

FIG. 1. Total electron-ion recombination cross sections for the F^{6+} ion, through the $1s^2 2p6l$ resonances. (a) Distorted-wave calculation without interference between DR and RR. The dashed-line curve represents the RR recombination. (b) Distorted-wave calculation including interference between DR and RR. (c) *R*-matrix calculation.

tronic recombination process. The last term in this expression is responsible for the asymmetric shape of the resonances.

Combining Eqs. (3), (4), and (7), the total distorted-wave recombination cross section in the presence of an isolated resonance may be expressed as

$$\sigma^R_{j\to i}=\sigma^{\rm RR}_{j\to i}+\sigma^{\rm DR}_{j\to i}+\sigma^{\rm RR}_{j\to i}B^a_n\left[\frac{2q^n_{ij}\epsilon_n+B^a_n-2}{\epsilon^2_n+1}\right], \quad (10)$$

where $\sigma^{\rm RR}_{j\to i}$ and $\sigma^{\rm DR}_{j\to i}$ are the RR and DR cross sections from i to j, respectively:

$$\sigma^{\rm RR}_{j\to i}=\frac{g_i}{2g_j}\frac{8\pi^2}{k^3}|\langle\psi_j|D|\psi_i\rangle|^2, \quad (11)$$

$$\sigma^{\rm DR}_{j\to i}=\frac{g_i}{2g_j}\frac{8\pi^2}{k^3}\left|\frac{\langle\psi_j|V|\phi_n\rangle\langle\phi_n|D|\psi_i\rangle}{\Delta_n+i\Gamma_n/2}\right|^2, \quad (12)$$

the Fano line-profile parameter [18] is defined as

$$q^n_{ij}=\frac{\langle\psi_j|V|\phi_n\rangle\langle\phi_n|D|\psi_i\rangle}{\langle\psi_j|D|\psi_i\rangle\dfrac{A^a_{n\to j}}{2}}, \quad (13)$$

B^a_n is the autoionization branching ratio given by $B^a_n=A^a_{n\to j}/\Gamma_n$, and $\epsilon_n=\Delta_n/\Gamma_n/2$.

The presence of the variable ϵ_n in Eq. (10) produces the asymmetry of the peaks, since this variable changes the sign at energies below and above the center of the peak, leading to a different interference effect at each side of the peak. If we neglect the last term in Eq. (7) coming from third-order perturbation theory, the last two terms inside the brackets in Eq. (10) disappear. In addition, the entire last term of Eq. (10) vanishes on energy averaging the recombination cross section.

The distorted-wave approximation presented here, which includes interference effects only between the DR and RR processes (i.e., resonance-background interferences), is valid for resonances having small values of the principal quantum numbers *n*. For extension to higher *n*, the treatment has to be generalized to allow overlapping resonances (i.e., resonance-resonance interferences). Such a treatment through the use of the projection operator formalism has recently been given by Robicheaux *et al.* [20] and Griffin *et al.* [21] for the case of DR in the presence of an electric field. The resonance energies, bound and continuum wave functions, matrix elements, and rates needed to evaluate the above equations for the total recombination cross section are calculated using the AUTOSTRUCTURE program [22].

III. TOTAL CROSS-SECTION RESULTS FOR F^{6+}

In an earlier paper [23], distorted-wave calculations for the complete dielectronic recombination spectrum of F^{6+} were compared with the experimental data obtained using the Aarhus University tandem accelerator, showing very good agreement. With the advent of new techniques for the lowering of the transversal temperature in the ion storage ring devices [24], considerable higher-resolution measurements of DR are now possible. In this paper we focus on the first two peaks of Fig. 5 of that earlier paper. With the increase in accuracy of the cooler-ring devices, experiments are able to resolve the structure of these peaks, missed in the earlier experiment.

Results of the total recombination cross section through the $1s^2 2p6l$ resonances in F^{5+} are presented in Fig. 1, while recombination through the $1s^2 2p7l$ resonances is presented in Fig. 2. For each of these figures we have calculated the cross sections using the perturbative distorted-wave method [(a) and (b)] and the nonperturbative *R*-matrix method (c). In part (a) of these figures, the calculation neglects interference between radiative and dielectronic recombination. In order to show the separate contribution of each process, the radiative recombination is shown in the dashed curves. In Fig. 2 the

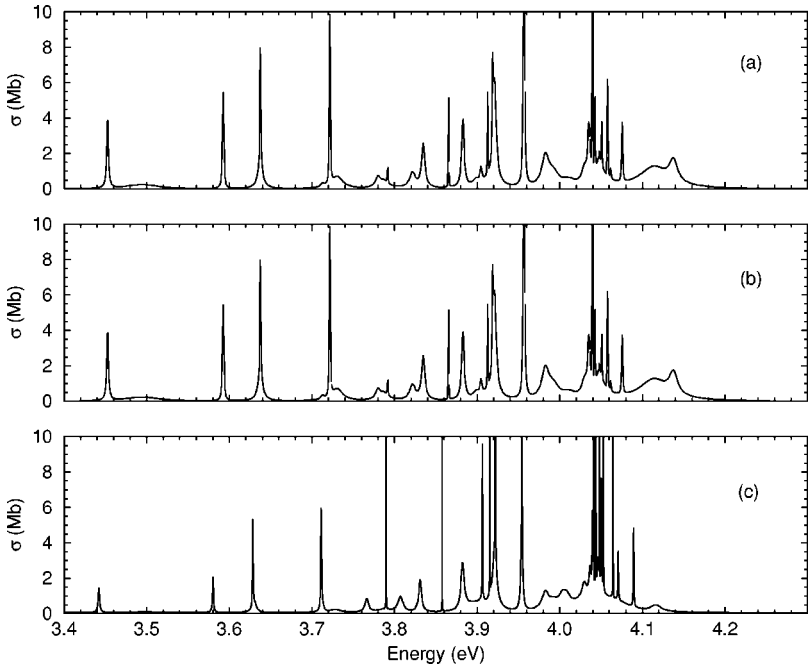

FIG. 2. Total electron-ion recombination cross sections for the F^{6+} ion, through the $1s^2 2p7l$ resonances. (a) Distorted-wave calculation without interference between DR and RR. (b) Distorted-wave calculation including interference between DR and RR. (c) *R*-matrix calculation.

RR curve coincides with the axis. In part (b) the curves include the quantum interference between the two processes. All the calculations have been performed in intermediate coupling, and we have shifted the calculated energies of the $1s^2 2s\,^2S_0$, $1s^2 2p\,^2P_{1/2}$, and $1s^2 2p\,^2P_{3/2}$ levels of the Li-like F^{6+} ion, in order to agree with the experimental values [25].

We have included in the three-level *R*-matrix calculation the $1s^2 2s$ and $1s^2 2p$ configurations of the recombining F^{6+} ion. This Breit-Pauli close-coupling calculation includes configuration interaction between all the levels associated with the $1s^2 2snl$ and $1s^2 2pnl$ configurations of the recombined F^{5+} ion. The *R*-matrix method also includes configuration interactions between the resonances and the continuum states associated with the recombining ion configurations. We have not included radiation damping in the *R*-matrix calculations, since for this low-*Z* ion the resonance widths are completely dominated by the autoionization width.

In the distorted-wave calculations through the $1s^2 2p6l$ resonances, we have included configuration interaction between the F^{5+} ground configuration $1s^2 2s^2$ and the $1s^2 2s2p$, $1s^2 2p^2$, $1s^2 2pnl$, and $1s^2 2s6l$ configurations. For the recombination through the $1s^2 2p7l$ resonances, we had to cut back some of the configuration interactions, neglecting the higher l levels of the configurations $1s^2 2p3l$ and $1s^2 2p4l$, and we neglect also the $1s^2 2s6l$ configuration. On the other hand, we added configuration interactions with the $1s^2 2p7l$ and $1s^2 2s7l$ configurations. Radiative transitions from the autoionizing $1s^2 2pnl$ levels have been calculated to all the lower levels, and we also have included cascades (radiative transitions between the autoionizing levels). The importance of radiation damping can be easily estimated by using the distorted-wave method, and we found that these effects are negligible.

The best candidates for the investigation of interference effects on the total recombination are, in general, the low-energy peaks. In this energy range, both the radiative and dielectronic recombination have a large cross section. Comparison between Fig. 1(a) and Fig. 1(b) shows that both results are almost identical. There is a small difference between the calculations that include and neglect the interferences between DR and RR at the very low-energy range (below 0.1 eV). These effects are so small that they might not be observed even in the high-resolution ion storage ring experiments.

Either for Fig. 1 or for Fig. 2, comparisons between the distorted-wave and *R*-matrix results show a reasonable agreement. The energy position of the resonances at this resolution is very sensitive to the configuration interactions included in the calculations. The similarity in the shape of the resonances obtained by using both methods indicates that resonance-background interferences are strongly suppressed. Therefore, the differences between the distorted-wave and *R*-matrix results can be assigned to the greater configuration interaction included in the *R*-matrix calculations.

IV. TOTAL RECOMBINATION RESULTS FOR F^{6+} NEAR ZERO ENERGY

Beginning with studies on U^{28+} [26,27], ion-beam experiments have reported unexpectedly large total recombination rates near zero energy. For example, in Au^{25+} [28] the measured total recombination rate is found to be over 300 times larger than the theoretical predictions of the radiative recombination rate. Experimental studies on Au^{49+}, Au^{50+}, and Au^{51+} [29] have shown that the absence or presence of low-energy dielectronic recombination resonances plays a significant role in the overall strength of the zero energy total recombination rate.

The total recombination cross section and rate for F^{6+} near zero energy are examined in detail in Fig. 3. The total recombination and radiative recombination cross sections are shown in Fig. 3(a). The main peaks at 0.031 eV and 0.040 eV correspond to the $1s^2 2p6p\,^3P_1$ and $1s^2 2p6p\,^3P_2$ resonance levels of F^{5+}. The $1s^2 2p6p\,^3P_1$ resonance has an especially large width extending into the near zero energy

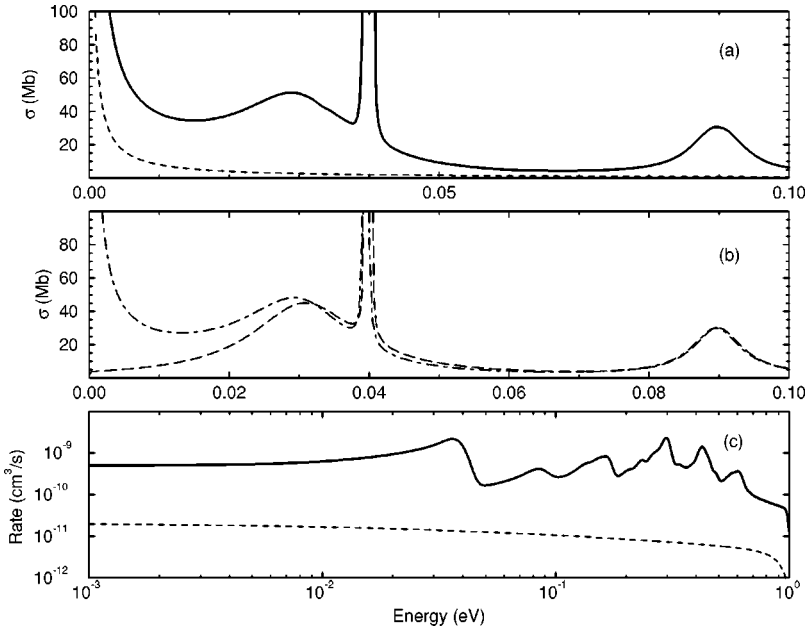

FIG. 3. Total electron-ion recombination for the F^{6+} ion, through the $1s^2 2p 6p$ resonances, near zero energy. (a) Total electron-ion recombination cross section (solid line) and RR cross section (dashed line). (b) DR cross section. Long-dashed line: calculated by using $\langle \sigma^{\mathrm{DR}} \rangle \Delta E/2\pi \times L(E_n)$ [Eq. (14)]; dot-dashed line: calculated by using Eq. (12). (c) Total recombination rate coefficient (solid line) and RR rate coefficient (dashed line).

region. At 0.01 eV the total recombination cross section is five times the radiative recombination cross section. As one moves to even lower energies, the total recombination cross section remains much larger than the radiative recombination. According to Eqs. (11) and (12), both the RR and DR cross sections have the same $1/k^3$ factor in front, thus both contributions increase at the same rate for low energies. If we express Eqs. (11) and (12) in terms of continuum wave functions normalized to $1/\sqrt{k}$ times a sine function, the resulting bound-free radiative and autoionization matrix elements are somewhat independent of energy. The resulting cross sections vary as $1/k^2$.

The DR cross section is, in general, sharply peaked around the resonance energies E_n, and there are many peaks within a small energy interval. In most of the theoretical calculations of DR, an average procedure [30] is applied. The DR cross section is averaged over an energy bin of size ΔE. So long as this bin size is chosen to be much smaller (at least a factor of 10 or more) than the actual experimental beam width, such an averaging procedure will contain exactly the same information as the original σ^{DR}. Thus, the bin-averaged dielectronic cross-section is defined as

$$\begin{aligned}\langle \sigma^{\mathrm{DR}}_{j\to i} \rangle &\equiv \frac{1}{\Delta E}\int_{E_n-\Delta E/2}^{E_n+\Delta E/2} \sigma^{\mathrm{DR}}(E')\,dE' \\ &\approx \frac{g_i}{2g_j}\frac{8\pi^2}{k_n^3}|\langle \psi_j|V|\phi_n\rangle\langle \phi_n|D|\psi_i\rangle|^2 \\ &\quad \times \frac{1}{\Delta E}\int_{E_n-\Delta E/2}^{E_n+\Delta E/2}\frac{dE'}{\Delta_n^2+\Gamma_n^2/4} \\ &\approx \frac{g_i}{2g_j}\frac{8\pi^2}{k_n^3}|\langle \psi_j|V|\phi_n\rangle\langle \phi_n|D|\psi_i\rangle|^2 \frac{1}{\Delta E}\frac{2\pi}{\Gamma_n},\end{aligned} \tag{14}$$

where $k_n = \sqrt{2E_n}$. The bin-averaged dielectronic recombination cross section fails at very low energies. At low energies the $1/k^2$ dependence of the DR cross section can no longer be assumed to be a constant over the bin width. To illustrate the error that could arise in using the bin-averaged DR cross section, we write

$$\sigma^{\mathrm{DR}}_{j\to i} \approx \langle \sigma^{\mathrm{DR}}_{j\to i} \rangle \frac{\Gamma_n \dfrac{\Delta E}{2\pi}}{\Delta_n^2 + \left(\dfrac{\Gamma_n}{2}\right)^2} = \langle \sigma^{\mathrm{DR}}_{j\to i} \rangle \frac{\Delta E}{2\pi} L(E_n), \tag{15}$$

where $L(E_n)$ is a Lorentzian-shape function, centered at the resonance energy E_n. In Fig. 3(b) is displayed the DR cross sections obtained by using the bin-averaged approximation of Eq. (15) (long-dashed curve) and the correct DR cross section using Eq. (12) (dot-dashed curve). The correct DR cross section at low energies is no longer a Lorentzian-shape curve. As seen in Fig. 3(a), in the presence of a resonance close to threshold, the separation of the RR from the total recombination cross section is not straightforward. It is interesting to note that the use of the bin-averaged approximation at low energies is erroneous, no matter how far the resonances are placed from the threshold. In fact, every DR peak would give a nonzero contribution at very low energy, and neglecting this contribution could lead to serious underestimation of the total recombination. Finally, we note that in all of our previous work on dielectronic recombination with and without interference effects we have made use of Eq. (12) rather than Eq. (15).

The total and radiative recombination rates are shown in Fig. 3(c). The rates are calculated by folding the total and radiative recombination cross sections with a double Maxwellian velocity distribution. We use $kT_{\|} = 0.1$ meV and $kT_{\perp} = 0.01$ eV, which are near the limit of current experimental resolution [9]. The total recombination rate is about 30 times larger than the radiative recombination rate at an energy of 0.001 eV. We note that a total recombination rate using the energy-averaged dielectronic recombination cross section would be very close to the total rate curve shown in Fig. 3(c). The small difference is due to the relatively large

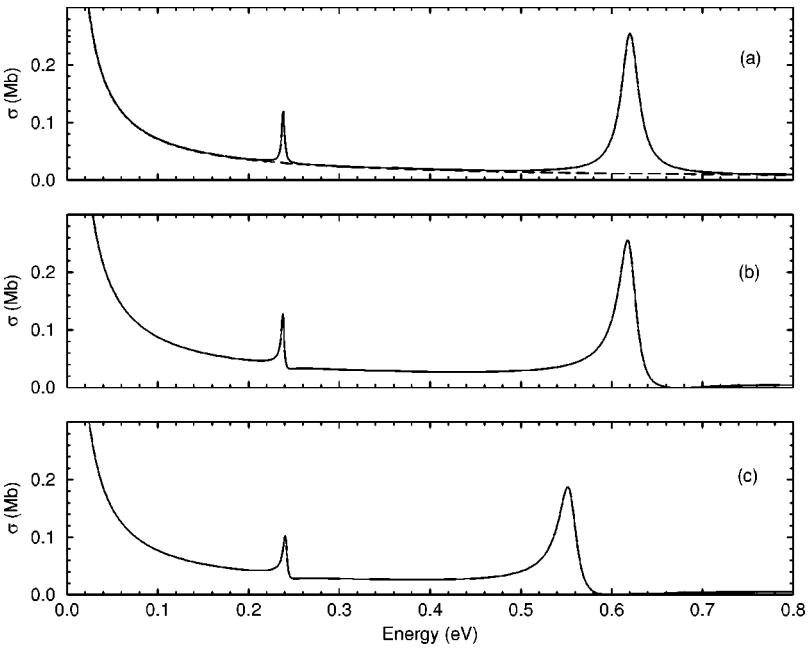

FIG. 4. Distorted-wave calculation of the partial recombination cross sections for the F^{6+} ion, through the $1s^22p6l$ resonances, to the $1s^22s^2\,{}^1S_0$ level. (a) Distorted-wave calculation without interference between DR and RR. The dashed-line curve represents the RR recombination. (b) Distorted-wave calculation including interference between DR and RR. (c) *R*-matrix calculation.

experimental resolution. If the temperatures in the double Maxwellian velocity distribution are reduced an order of magnitude, then the effect of using an energy-averaged dielectronic recombination cross section is very noticeable. On the other hand, one could stay with the current experimental resolution and move to higher charge states in the Li isoelectronic sequence. Then the differences between the correct low-energy cross section and an energy-averaged cross section would also grow quite large.

Finally, we warn the reader that the effect of low-energy dielectronic resonances on the total recombination rate is not the end of the story. Even for bare ions, where no dielectronic resonances are able to contribute, there still remains a substantial discrepancy between observed total recombination rates and theoretical predictions of the radiative recombination rate [31].

V. PARTIAL CROSS-SECTION RESULTS FOR F^{6+}

Promising candidates for the observation of the breakdown of the independent-processes approximation in the partial recombination of F^{6+} are the following processes:

$$\begin{aligned} e^- + F^{6+}(1s^22s) &\rightarrow F^{5+}(1s^22pnl) \\ &\rightarrow F^{5+}(1s^22s^2\,{}^1S_0) + h\nu_1, \\ e^- + F^{6+}(1s^22s) &\rightarrow F^{5+}(1s^22pnl) \\ &\rightarrow F^{5+}(1s^22s2p\,{}^3P_{0,1,2}) + h\nu_2, \quad (16) \\ e^- + F^{6+}(1s^22s) &\rightarrow F^{5+}(1s^22pnl) \\ &\rightarrow F^{5+}(1s^22s2p\,{}^1P_1) + h\nu_3, \end{aligned}$$

where n is 6 and 7 for the $1s^22pnl$ intermediate autoionizing configurations.

In Fig. 4 we present the partial recombination cross section into the $1s^22s^2\,{}^1S_0$ final level of the recombined F^{5+} ion. The recombination cross section obtained by adding the DR and RR, without interference, is shown in Fig. 4(a). In order to appreciate the separate contribution of each process, the RR is displayed in the dashed curve. In Fig. 4(b) is shown the recombination cross section including the interferences. In both figures, the calculations were performed by using the distorted-wave method. In Fig. 4(c) is displayed the cross section obtained by using the *R*-matrix calculations. This method, unlike the perturbative method, includes the interferences implicitly and it is not easy to analyze them separately.

Most of the contribution from the $1s^22p6l$ resonances has disappeared, since they cannot dipole radiate to the ground configuration. However, two peaks appear in the recombination spectra. The first peak at 0.24 eV is produced by DR through the $1s^22p6d\ {}^3D_1$ autoionizing level, and the second peak at 0.62 eV is produced through the $1s^22p6d\ {}^1P_1$ autoionizing level. It appears that the dominant stabilization pathway is due to weak configuration-interaction mixing between the $^1S_0$ ground level and $1s^22p6p(J=0)$ levels, and strong radiative coupling between the $1s^22p6d$ and $1s^22p6p$ levels. These peaks result in the emission of approximately 157 eV x-ray light. The asymmetry of the peaks resulting when the interference is included is quite noticeable. Comparison between Fig. 4(b) and Fig. 4(c) shows a reasonable agreement, both in the position and the shape of the resonances, between the distorted-wave and the *R*-matrix results. This partial recombination is an example of a weak transition having strong interference. Since the radiative transitions are allowed only by configuration interaction, extensive calculations are needed to account for the different correlation effects. The position and shape of the peaks seem to be very sensitive to these interactions.

Figure 5 shows the partial recombination cross section to the $1s^22s2p\,{}^3P_2$ level. Figure 5(a) shows the distorted-wave calculation of the recombination without the interference of DR and RR, i.e., the separate addition of these two independent processes. The dashed curve represents the RR process alone. Figure 5(b) shows the distorted-wave calculation of the recombination including the interference, and in Fig. 5(c)

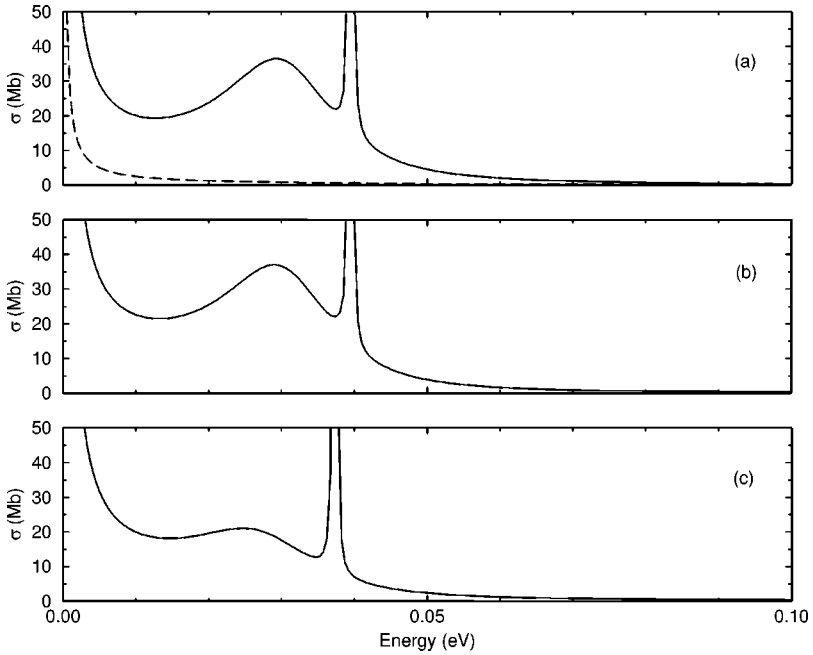

FIG. 5. Distorted-wave calculation of the partial recombination cross sections for the F^{6+} ion, through the $1s^2 2p 6l$ resonances, to the $1s^2 2s 2p\ ^3P_2$ level. (a) Distorted-wave calculation without interference between DR and RR. The dashed-line curve represents the RR recombination. (b) Distorted-wave calculation including interference between DR and RR. (c) *R*-matrix calculation.

is shown the *R*-matrix calculation. The two main peaks observed in the figures, at 0.031 eV and 0.040 eV, correspond to the recombination through the $1s^2 2p 6p\ ^3P_1$ and $1s^2 2p 6p\ ^3P_2$ levels, respectively. This particular partial recombination cross section dominates the total recombination cross section for these two resonances. If we compare the height of the partial cross section of the $1s^2 2p 6p\ ^3P_1$ resonance in Fig. 5(a) with the height of the total cross section of the same resonance in Fig. 1, we see that the ratio is about 0.75. Since for low-*Z* ions the dielectronic recombination is roughly proportional to the radiative rate, we can verify the figure heights by taking the ratio of the partial to total radiative rates. The ratio of the partial radiative rate to the total radiative rate is 75% for the $^3P_1$, while the ratio for the $^3P_2$ is 63%. As expressed in Eq. (10), a peak must have a small Fano parameter in order to show a noticeable asymmetric shape. A small Fano parameter can be obtained with large autoionization and photoionization rates and a small radiative transition rate [see Eq. (13)]. The first peak of Fig. 5 has a very high autoionization rate ($A^a_{n\to j}=2.8\times10^{14}$ Hz), a relatively high photoionization cross section ($\sigma^{\omega}_{i\to j}=1.7\times10^{-20}$ cm^2), but a radiative transition rate ($A^r_{n\to i}=8.3\times10^9$ Hz) that is not small enough to produce a very small Fano parameter ($q^n_{ij}=-11$). The second peak has an autoionization rate coefficient of $A^a_{n\to j}=1.3\times10^{11}$ Hz and a Fano parameter $q^n_{ij}=-239$. This large parameter produces a symmetric Lorentzian shape in the resonance, and the resulting shape of this particular resonance is very similar to that obtained by neglecting the interference.

The general features in the recombination spectrum shown in Fig. 5 depend on the autoionization and radiative rates and one might expect that configuration-interaction effects would not change the rates by such an amount so as to change the shape of the peaks. However, as in the previous example of transitions to the ground level, the results are very sensitive to the structure calculation and the correlations included. The separation between the peaks is small and slight changes in the energies result in large changes in the final curves. Within the degree of accuracy in our calculations, the first resonances at very low energy might actually be located below the threshold, and therefore would vanish from the recombination spectra. We also investigated the partial recombination to the levels $1s^2 2s 2p\ ^3P_{0,1}$ and $^1P_1$, but they did not show any interesting interference effects.

Noticeable interference effects for the recombination through the $1s^2 2p 7l$ intermediate autoionizing levels have been found only for the partial recombination to the ground $^1S_0$ level, and they are displayed in Fig. 6. The distorted-wave calculations are very sensitive to configuration interaction, especially correlations between the $1s^2 2p 7l$ levels (without these interactions, the peaks vanish). The curves of Fig. 6(a) and Fig. 6(b) were calculated using the distorted-wave method, and for Fig. 6(c) the *R*-matrix method was employed. In part (a) of the figure, the sum of the DR and RR cross sections, without interference, is shown, while part (b) shows the recombination cross section including the interferences. Configuration interaction between $1s^2 2p 7l$, $1s^2 2pnl'$ $(2\leqslant n\leqslant 6)$, $1s^2 2s 7l$, and $1s^2 2s 2l''$ has been included in the perturbative distorted-wave calculations. Comparison between Fig. 6(b) and Fig. 6(c) shows a reasonable agreement between the distorted-wave and the *R*-matrix results. For this case, the agreement for the position of the peaks is better than 0.05 eV. The shapes of the last two peaks (at 3.88 eV and 4.14 eV) are also the same for both calculations, but the rates, and in consequence the height of the peaks, are higher for the perturbative calculations. The transitions are very weak because they are only dipole-allowed through configuration interaction. In order to be measured, those partial recombination events which emit a photon having $h\nu\approx160$ eV must be selected.

VI. SUMMARY

Using both perturbative distorted-wave theory and nonperturbative *R*-matrix theory we have calculated the total and partial electron-ion recombination cross sections for the

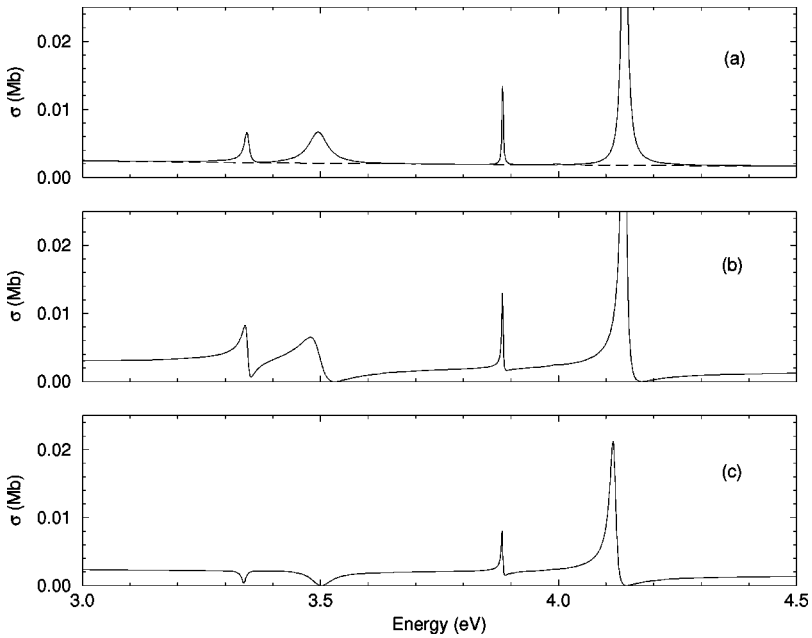

FIG. 6. Distorted-wave calculation of the partial recombination cross sections for the F^{6+} ion, through the $1s^2 2p7l$ resonances, to the $1s^2 2s^2\ ^1S_0$ level. (a) Distorted-wave calculation without interference between DR and RR. The dashed-line curve represents the RR recombination. (b) Distorted-wave calculation including interference between DR and RR. (c) *R*-matrix calculation.

ground state of F^{6+} in the vicinity of the $1s^2 2p6l$ and $1s^2 2p7l$ resonances. Quantum interference effects between the radiative and dielectronic recombination processes are found to be largest for the partial recombination cross section into the ground $1s^2[2s^2+2p^2]\ ^1S_0$ final recombined level of F^{5+}.

The partial recombination cross section into the ground $^1S_0$ level consists of very weak resonances having radiative decays which are produced mainly through configuration-interaction effects. These resonances are buried under other stronger resonances and are not distinguishable in the total recombination spectra. However, they show interesting asymmetric shapes that could be observed in experiments in which the final recombination state is selected. The partial recombination cross section into the $1s^2 2s2p\ ^3P_2$ level is a dominant pathway for some resonances, but shows a very small asymmetric shape.

We have to mention some possible qualifications to our conclusions. First, the weak partial recombination structures are very sensitive to correlation effects. Even for this simple Li-like ion, extensive calculations must be employed in order to accurately find both the energy position and shape of the peaks. Second, the peaks that could show some interference effects in the total recombination are located very close to the threshold and have small energy separations. This means that knowledge of the exact position of the peaks is crucial for an accurate calculation of the cross section. The cross-section results shown here may serve as a convenient focus for future experiments attempting to observe the breakdown of the independent-processes approximation. The analysis of the factors responsible for the interference effects can help in the theoretical search for other cases. As we show in this paper, the interference effects are not necessarily limited to highly charged high-*Z* ions or to special cases.

ACKNOWLEDGMENTS

The authors wish to thank F. Robicheaux for stimulating conversations. D.M.M. and M.S.P. were supported in part by the U.S. Department of Energy under Contract No. DE-FG05-96ER54348 with Auburn University, and Grant No. DE-FC02-91ER75678 with Alabama EPSCoR.

[1] M.S. Pindzola, N.R. Badnell, and D.C. Griffin, Phys. Rev. A **46**, 5725 (1992).
[2] V.L. Jacobs, J. Cooper, and S.L. Haan, Phys. Rev. A **36**, 1093 (1987).
[3] K.J. LaGattuta, Phys. Rev. A **36**, 4662 (1987); **38**, 1820 (1988); **40**, 558 (1989).
[4] S.L. Haan and V.L. Jacobs, Phys. Rev. A **40**, 80 (1989).
[5] N.R. Badnell and M.S. Pindzola, Phys. Rev. A **45**, 2820 (1992).
[6] S.N. Nahar and A.K. Pradhan, Phys. Rev. Lett. **68**, 1488 (1992): Phys. Rev. A **49**, 1816 (1994).
[7] F. Robicheaux, T.W. Gorczyca, M.S. Pindzola, and N.R. Badnell, Phys. Rev. A **52**, 1319 (1995).
[8] T.W. Gorczyca, F. Robicheaux, M.S. Pindzola, and N.R. Badnell, Phys. Rev. A **54**, 2107 (1996).
[9] S. Mannervik, D. DeWitt, L. Engström, J. Lidberg, E. Lindroth, R. Schuch, and W. Zong, Phys. Rev. Lett. **81**, 313 (1998).
[10] T.W. Gorczyca, M.S. Pindzola, F. Robicheaux, and N.R. Badnell, Phys. Rev. A **56**, 4742 (1997).
[11] S. Schippers, T. Bartsch, C. Brandau, J. Linkemann, A. Müller, A. Saghiri, and A. Wolf, Hyperfine Interact. **114**, 273 (1998).
[12] D.A. Knapp, P. Beiersdorfer, M.H. Chen, J.H. Scofield, and D. Schneider, Phys. Rev. Lett. **74**, 54 (1995).
[13] M.S. Pindzola, F. Robicheaux, N.R. Badnell, M.H. Chen, and M. Zimmermann, Phys. Rev. A **52**, 420 (1995).

[14] M.J. Seaton, Proc. R. Soc. London, Ser. A **218**, 400 (1953).
[15] P.G. Burke and K.A. Berrington, *Atomic and Molecular Processes: An R-matrix Approach* (IOP, Bristol, 1993).
[16] K.A. Berrington, W.B. Eissner, and P.H. Norrington, Comput. Phys. Commun. **92**, 290 (1995).
[17] N.R. Badnell, T.W. Gorczyca, and A.D. Price, J. Phys. B **31**, L239 (1998).
[18] U. Fano, Phys. Rev. **124**, 1866 (1961); U. Fano and J.W. Cooper, *ibid.* **137**, A1364 (1965).
[19] H.P. Kelly and R.L. Simons, Phys. Rev. Lett. **30**, 529 (1973).
[20] F. Robicheaux, M.S. Pindzola, and D.C. Griffin, Phys. Rev. Lett. **80**, 1402 (1998).
[21] D.C. Griffin, D.M. Mitnik, M.S. Pindzola, and F. Robicheaux, Phys. Rev. A **58**, 4548 (1998).
[22] N.R. Badnell, J. Phys. B **19**, 3827 (1986); **30**, 1 (1997).
[23] L.H. Andersen, G-Y. Pan, H.T. Schmidt, M.S. Pindzola, and N.R. Badnell, Phys. Rev. A **45**, 6332 (1992).
[24] H. Danared, G. Andler, L. Bagge, C.J. Herrlander, J. Hilke, J. Jeansson, A. Källberg, A. Nilsson, A. Paál, K.G. Rensfelt, U. Rosengård, J. Starker, and M. af Ugglas, Phys. Rev. Lett. **72**, 3775 (1994).
[25] C.E. Moore, *Atomic Energy Levels*, Natl. Bur. Stand. Ref. Data Ser., Natl. Bur. Stand. (U.S.) (U.S. GPO, Washington, DC, 1971), Vol. I.
[26] S. Schennach, A. Müller, M. Wagner, J. Haselbauer, O. Uwira, W. Spies, E. Jennewein, R. Becker, M. Kleinod, U. Pröbstel, N. Angert, J. Klabunde, P.H. Mokler, P. Spädtke, and B. Wolf, in *Atomic Physics of Highly Charged Ions*, edited by E. Salzborn, P.H. Mokler, and A. Müller (Springer, Berlin, 1991), p. 205.
[27] D.M. Mitnik, M.S. Pindzola, F. Robicheaux, N.R. Badnell, O. Uwira, A. Müller, A. Frank, J. Linkemann, W. Spies, N. Angert, P.H. Mokler, R. Becker, M. Kleinod, S. Ricz, and L. Empacher, Phys. Rev. A **57**, 4365 (1998).
[28] A. Hoffknecht, O. Uwira, S. Schennach, A. Frank, J. Haselbauer, W. Spies, N. Angert, P.H. Mokler, R. Becker, M. Kleinod, S. Schippers, and A. Müller, J. Phys. B **31**, 2415 (1998).
[29] O. Uwira *et al.*, Hyperfine Interact. **108**, 149 (1997).
[30] Y. Hahn, Adv. At. Mol. Phys. **21**, 142 (1985).
[31] H. Gao, R. Schuch, W. Zong, E. Justiniano, D.R. DeWitt, H. Lebius, and W. Spies, J. Phys. B **30**, L499 (1997).